ADVANCED MATERIALS INTERFACES
www.advmatinterfaces.de

Enhanced Boiling Heat Transfer Performance on Microstructured Silicate Glass Surfaces Derived from Inorganic Polymer-Based Soft Lithography

Hyunwoo Noh, Jin-Oh Kim, Dong-Hwi Kim, Hyun Sun Park, Yoon-Ho Hwang, Moo Hwan Kim, and Dong-Pyo Kim**

Boiling is a vigorous phase change phenomenon from liquid to vapor and large amount of heat transfer is accompanied due to the latent heat of vaporization. Therefore, boiling is widely utilized in industrial fields such as power plant, desalination plant, material processing, refrigeration, and electric device cooling.[1–9] In particular, the effective cooling in an integrated heat exchange system is required to consider fast heat removal, high heat transfer efficiency, and low thermal stress.[4] Meanwhile, the boiling behavior is dependent of surface conditions. It was reported that surface structure affects boiling heat transfer by changing nucleation behavior and bubble dynamics.[1,10–14] For example, porous surface acted as vapor cavities induced vigorous bubble generation and enhanced heat transfer performance during boiling.[12,13] In addition, surface chemistry also has an influence on boiling performance, as the different wettability on hydrophobic and hydrophilic surfaces drastically caused the change of bubble motion.[15,16] Moreover, it was feasible that control of both surface chemistry and geometry further enhanced the boiling heat transfer by inducing early bubble nucleation at lower temperature and providing liquid path through surface structures, leading to increase the bubble generation rate.[11] An advanced surface modification technique allowed to demonstrate the synergic effect.[11,17]

In practical, the boiling heat transfer application requires resistant materials at diverse harsh conditions, including high temperature durability. Therefore, silicon and metals have been mostly employed.[10,13,18–21] However, these materials need complicated fabrication with high cost for surface modification.[10,11,17] It is desirable to facilitate manufacturing the surface textures with excellent cooling performance by adopting new material with superior processability in terms of cost, formability, and durability.[22,23]

Si-based preceramic resin has been known for precursors of nonoxide ceramics such as SiC and Si_3N_4 under high temperature pyrolysis.[24,25] Recently, mild conversion process to oxide ceramics such as SiO_2 and SiCxOy phase was reported by room temperature hydrolysis of the consolidated preceramic polymers.[26] Therefore, it is appeared that a viscous allylhybridopolycarbosilane (AHPCS) polymer as a precursor of hydrophilic silicate glass is suitable for heat transfer applications since the heat and solvent resistance could be attained by step-wise crosslinking consolidation and hydrolysis steps.[25,26] In addition, the AHPCS precursor is readily compatible with various micromolding and printing techniques to fabricate the 2D and 3D ceramic microstructural features on various substrates.[24,27,28]

Herein, we develop the fabrication method of oxide ceramic like micropillar structures by inorganic polymer-based soft lithography and subsequent hydrolysis step to demonstrate efficient performance of boiling heat transfer surface. First, versatile AHPCS derived micropillar structures were fabricated by micromolding techniques. Their surface chemistry was controlled to design the wetting characteristics with hydrophilic, hydrophobic, or Janus wetting (having both hydrophilic and hydrophobic) surfaces in a selective manner. Moreover, the 3D macroporous network was additionally embedded into the ceramic like micropillar structures by packing sacrificial polystyrene (PS) bead templates (see **Scheme 1**). Pool boiling experiments were conducted with flat and microstructured surfaces to determine comparatively the heat transfer efficiency. Eventually, this work demonstrates that the designed surfaces in geometry and chemistry greatly improved the cooling efficiency beyond the material limitation. It is very likely to have potential that this inorganic polymer-based soft lithography technique enables to employ versatile cooling patterns on the surface of electronic components in a cost- and labor-saving manner compared to the silicon and metal based techniques.

Liquid type of AHPCS precursor easily formed versatile micropillar structures from soft lithography technique. Scheme 1 describes fabrication processes of various AHPCS micropillar structures on flat silicon substrates using a polydimethylsiloxane (PDMS) mold. The PDMS stamp is readily demolded from the solidified AHPCS patterns after curing step to prepare well-defined micropillar structures with 55 μm cylindrical diameter, 25 μm height, and 25 μm pitch distance (**Figure 1**a–c).

H. Noh
Department of Mechanical Engineering
Pohang University of Science and Technology (POSTECH)
Pohang 37673, Republic of Korea
J.-O. Kim, D.-H. Kim, Y.-H. Hwang, Prof. D.-P. Kim
National Center of Applied Microfluidic Chemistry
Department of Chemical Engineering
Pohang University of Science and Technology (POSTECH)
Pohang 37673, Republic of Korea
E-mail: dpkim@postech.ac.kr
Prof. H. S. Park, Prof. M. H. Kim
Division of Advanced Nuclear Engineering
Pohang University of Science and Technology (POSTECH)
Pohang 37673, Republic of Korea
E-mail: hejsunny@postech.ac.kr

DOI: 10.1002/admi.201600507

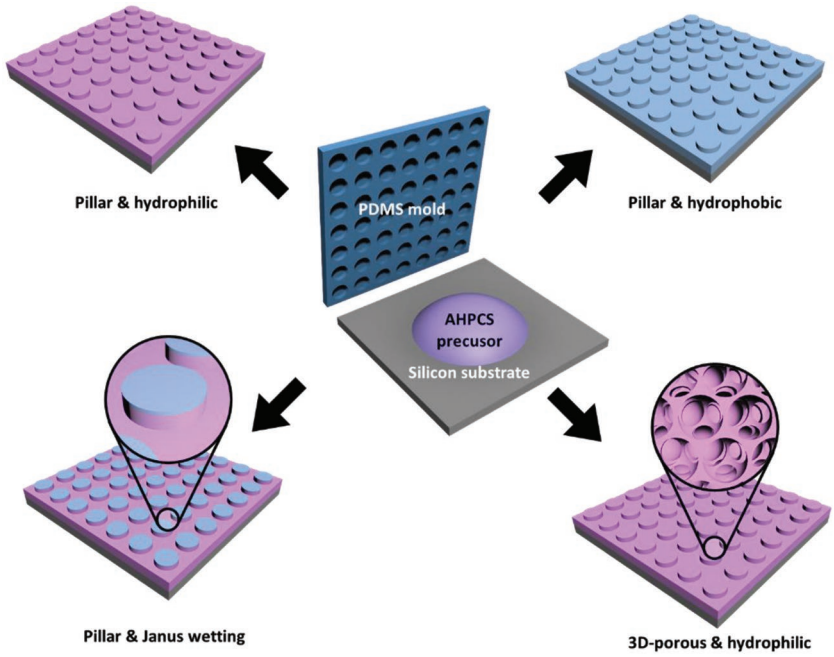

Scheme 1. Schematic illustration of the fabrication of AHPCS derived ceramic like micropillar structures with modified surface wettability as pillar and hydrophilic, pillar hydrophobic, pillar and Janus wetting, and 3D-porous and hydrophilic.

In our previous report, the preceramic AHPCS polymer was converted to hydrophilic silicate phase with SiCxOy chemical composition by hydrolytic phase conversion chemistry under basic condition at 70 °C,[26] as verified by the attenuated total reflectance (ATR) analysis (Figure S4, Supporting Information). The ATR spectrum showed that the Si–H peak (2150 cm^{-1}) was significantly decreased by hydrolyzing into Si—OH groups, while the Si—O—Si peak (1100 cm^{-1}) was newly appeared by forming from condensation between Si—OH groups. Note that this low temperature conversion to silicate oxide ceramic like phase did not cause any surface defects and cracks with nearly no shrinkage due to minimized molecular rearrangement, unlike high temperature pyrolytic conversion to SiC-based ceramics.[29] Moreover the long exposure to boiling water for 12 h did not form surface defect without property change, indicating sufficient thermal durability as expected (Figure S5, Supporting Information). The apparent contact angle of AHPCS derived flat surfaces changed from 94° of the polymeric phase to 54° after

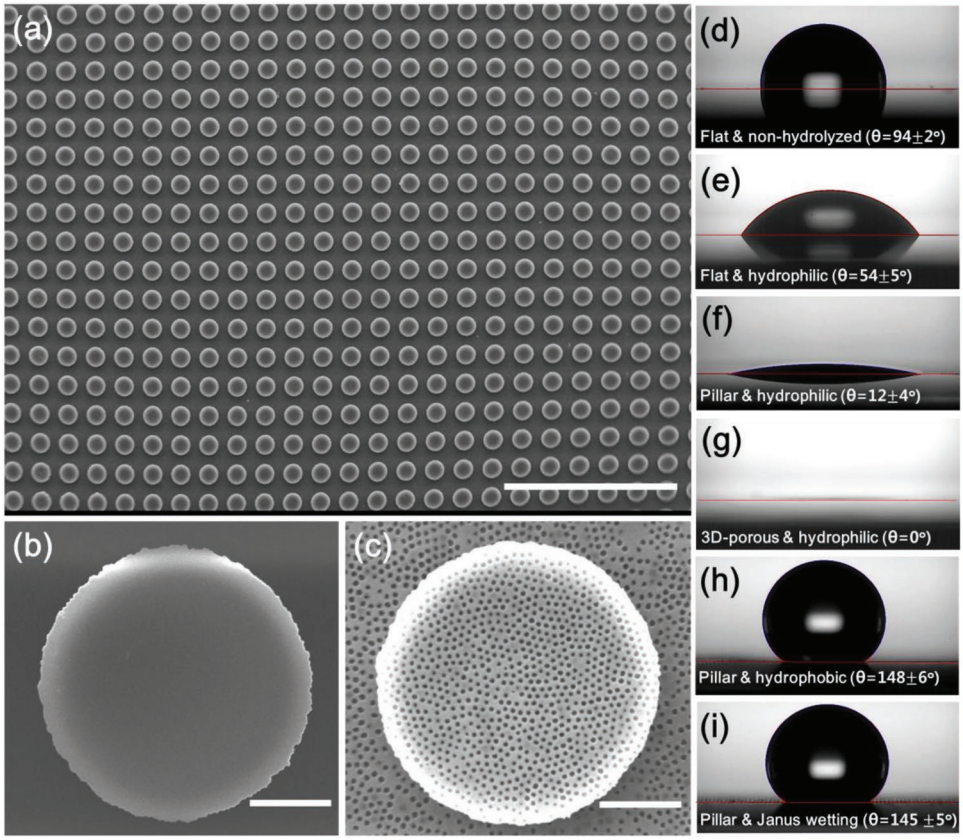

Figure 1. AHPCS derived micropillar (55 µm diameter, 25 µm height, and 25 µm pitch) structured surface. Scaning Electron Microscope (SEM) images of top view for a) large area of oxide ceramic like pattern (scale bar: 500 µm); b,c) nonporous and porous oxide ceramic like structure (scale bar: 15 µm); apparent contact angles of various ceramic like surfaces: d) flat and nonhydrolyzed, e) flat and hydrophilic, f) pillar and hydrophilic, g) 3D-porous and hydrophilic, (h) pillar and hydrophobic, and (i) pillar and Janus wetting.

hydrolysis (Figure 1d,e). In addition microstructures increased surface roughness and therefore further hydrophilic behaviors were observed (Figure 1f,g). The hydrolyzed AHPCS surface has Si—OH surface groups that are useful for further chemical modification by simple fluorination posttreatment via chemical vapor deposition of trichloro-(1H,1H,2H,2H-perfluorooctyl)-silane compound, as well documented,[30] resulting in hydrophobic surface with apparent contact angle 148° (Figure 1h).

Furthermore, the surface of micropillar cylinder was also modified to become a pillar and Janus wetting pattern with hydrophobic head and hydrophilic body, as described at Scheme S1 in the Supporting Information. Initially, the head of the hydrolyzed pillar structures was pressed with a flexible PDMS slab to protect from a contact of molten wax that was penetrated into the vacancy among the pillars by capillary effect and became solid on cooling. Then the exposed head by removal of the PDMS slab was selectively fluorinated, and the veiled bottom part of the hydrolyzed pillar reexposed the original hydrophilic surface when completely washed the wax out with toluene solution at 70 °C (Figure S6, Supporting Information). The pillar and Janus wetting surface retained hydrophobicity with 145° of apparent contact angle (Figure 1i) that is similar to 148° of the entirely fluorinated pillar structured surface.[31,32] However, the droplet impingement test showed quite different adhesion behavior (Figure S1, Supporting Information). The pillar and Janus wetting surface suspended the water droplet upon impinging, while the entirely fluorinated surface bounced and rolled the droplet with no pinning effect.[33] It indicates that the wetting dynamics of the chemically and geometrically modified surfaces is different from the only chemically modified surface, as consistent with the report.[11]

In addition, the oxide ceramic like micropillar structure embedded with 3D macroporosity was fabricated by using PS polymer beads (1.5 µm diameter) as sacrificial templates (Scheme S2, Supporting Information).[27,34,35] The PS beads in the suspension were induced to fill the microcavity of PDMS mold due to the capillary force. After solvent evaporation, the PDMS mold with close-packed PS beads was gently placed on the spin-coated film of viscous AHPCS precursor that was readily infiltrated into the voids among the PS beads within few seconds. Subsequently, the AHPCS–PS beads composite micropillar structures were fabricated by peeling off the PDMS mold after solidifying the double bonds of the former AHPCS under UV radiation for 15 min. Eventually, the 3D-porous silicate pillar structure was successfully formed by a serial process of postcuring at 120 °C for 2 h, sacrificial step of the PS beads with toluene and hydrolysis step (Figure 1c and Figure S7 in the Supporting Information). Note that the contacted PS beads in the close-packed array rendered the open macroporous network structure with interconnected windows (Figure S7c–f, Supporting Information).

Now the fabricated three different micropillar silicate surfaces are ready for pool boiling experiments to determine the heat transfer performance. The samples were installed at the bottom of the test pool and heated by the electric joule heating method, as conducted in the previous work (Figures S2 and S3, Supporting Information).[11] As shown in **Figure 2**, when heat flux at 100 kW m^{-2} was identically applied to every surface, the bubble dynamics and the temperature distribution were monitored by a high speed camera and an IR thermometry, respectively.

Heat transfer in boiling situation is strongly dependent on bubble dynamics. According to a classical heat flux portioning model, heat transfer can be divided with three mechanisms: evaporation, quenching, and convection.[36] Gerardi et al. and Kim et al. compared the effect of each mechanism and verified that evaporation and quenching take most of heat transfer in boiling.[37,38] Correlations for evaporation and quenching heat

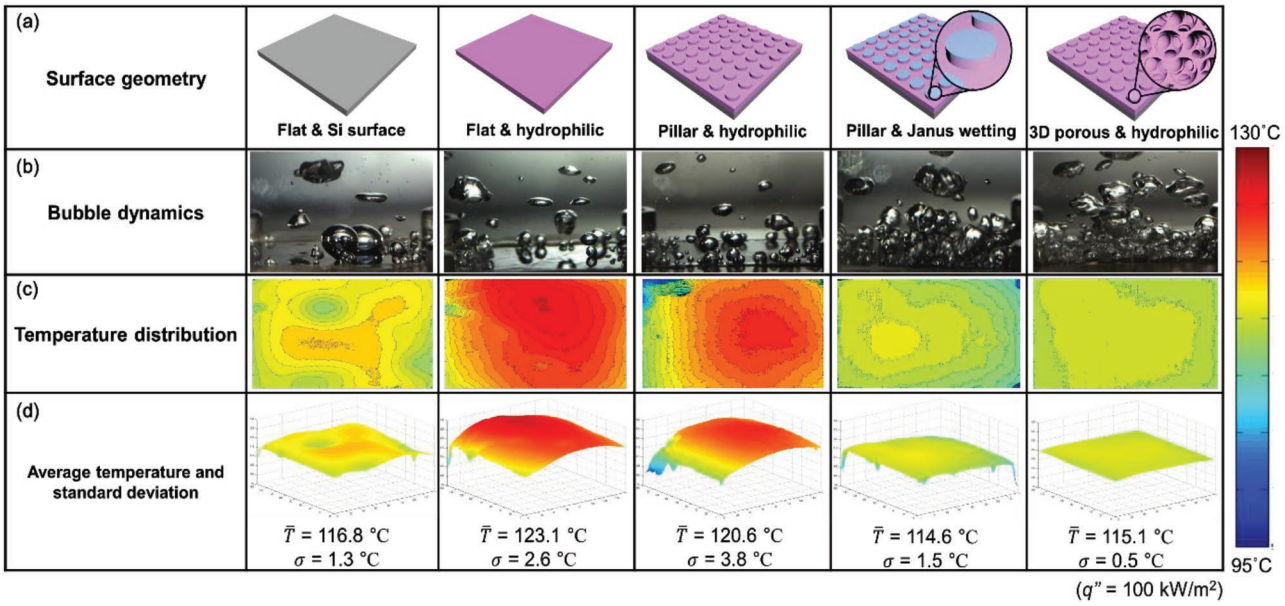

Figure 2. Comparative boiling characteristics of a) flat Si wafer and various AHPCS-derived silicate surfaces with different surface geometry and chemistry under heat flux of 100 kW m^{-2}. b) Bubble generation behavior (nucleation site and bubble diameter) captured by high speed camera. c) Temperature distribution and contour (1 °C difference/line) measured by high speed IR thermometry, color bar at the right side. d) 3D temperature distribution and statistical data (average temperature, standard deviation) for comparative cooling performances.

flux are below, and number of nucleation site (N_T), bubble departure diameter (D_b), and frequency (f_b) are most important parameters. They used quenching model of Han and Grifith[39]

$$q''_e = \frac{\pi}{6A}\rho_v h_{fg}\sum_{n=1}^{N_T}\left(f_{b,n}D_{b,n}^3\right) \quad (1)$$

$$q''_q = \frac{2\pi k_l\left(T_w - T_{sat}\right)}{A\sqrt{\pi\alpha_l}}\sum_{n=1}^{N_T}\left(D_{b,n}^2\left(\sqrt{t_{w,n}}f_{b,n}\right)\right) \quad (2)$$

where q''_e is the evaporative heat flux, q''_q is the quenching heat flux, A is the heating area, ρ_v is the density of vapor, h_{fg} is the enthalpy change from liquid to vapor, N_T is the total number of nucleation sites, f_b is the bubble frequency, k_l is the thermal conductivity of liquid, T_w is the wall temperature, T_{sat} is the saturation temperature, α_l is the thermal diffusivity of liquid, and t_w is the waiting time (time between bubble departure and next bubble generation).

From high speed visualization images shown in Figure 2b and Movie S1 in the Supporting Information, the heat transfer behaviors (nucleation site density, growth time, waiting time, frequency, and departure diameter) of various surfaces were investigated (**Figure 3**). The flat and hydrophilic surface had fewer nucleation sites (1.74 cm^{-2}) and lower bubble generation frequency (4.8 Hz) than the flat silicon surface (2.08 cm^{-2} and 19.0 Hz). Therefore, the heat transfer performance in AHPCS itself could be estimated as lower than Si although it has slightly larger bubble departure diameter (flat and hydrophilic: 4.54 mm/flat Si: 3.52 mm). As a result, at the same heat flux condition of 100 kW m^{-2}, the flat and hydrophilic surface represented the highest surface temperature (123.1 °C). However, although fabricated with the same material, the micropillar oxide ceramic like surfaces showed lower surface temperatures: 120.6 °C for the pillar and hydrophilic, 114.6 °C for the pillar and Janus wetting and 115.1 °C for the 3D-porous and hydrophilic surface. On these surfaces, much more nucleation sites were activated as can be seen from the nucleation site density and frequency results in Figure 3a,b (pillar and hydrophilic: 6.25 cm^{-2} and 25.1 Hz, pillar and Janus wetting: 55.56 cm^{-2} and 20.4 Hz, and 3D-porous and hydrophilic: 45.83 cm^{-2} and 128.2 Hz). Although departure diameters of microstructured surfaces represented smaller values than the flat and hydrophilic surface, the effect of diameter was overcome due to extremely increased nucleation site densities and frequencies.

Moreover, vigorous nucleation can also guarantee even temperature distribution through the surface. Heat transfer mainly occurs near the nucleation sites, and therefore uniformly existing nucleation sites on pillar and Janus wetting and 3D-porous and hydrophilic surfaces brought more cooling sites and prevented local temperature increment. As a result, little spatial temperature gradient with smaller number of contour and small standard deviation for temperature distribution were observed on those surfaces (Figure 2c,d and Movie S2 in the Supporting Information). Little temperature gradient derived by the uniform cooling effect has advantages for practical applications to reduce thermal stress and performance deterioration of electrical devices.[4]

To understand the cooling performances in detail, heat transfer coefficients (HTCs) and bubble nucleation

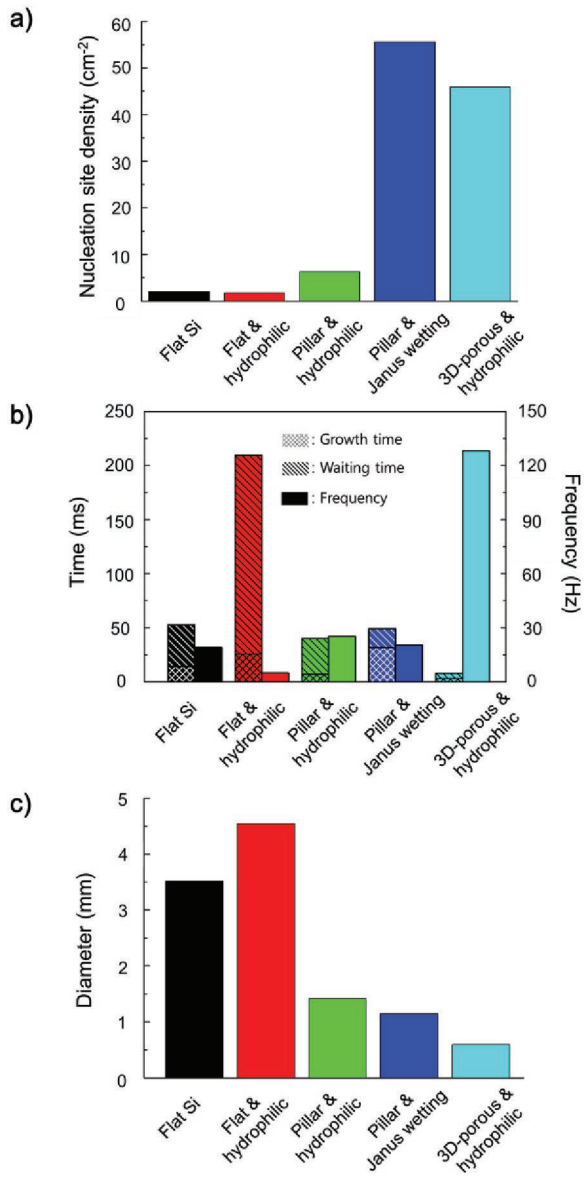

Figure 3. Bubble dynamics analysis: a) nucleation site density, b) growth time, waiting time, and frequency, and c) bubble departure diameter (■ flat Si, ■ flat and hydrophilic, ■ pillar and hydrophilic, ■ pillar and Janus wetting, and ■ 3D-porous and hydrophilic).

temperatures were comparatively determined (**Figure 4**). The HTC is defined as the ratio between the applied heat flux and the increased surface temperature, which is strongly related with cooling efficiency on boiling. In general, higher HTC is substituted with lower temperature increment at a same heat flux condition. The flat and hydrophilic surface had lower HTC (4.26 kW m^{-2} K^{-1}) than the flat Si wafer case (5.57 kW m^{-2} K^{-1}), while pillar and Janus wetting (6.81 kW m^{-2} K^{-1}) and 3D-porous and hydrophilic (6.57 kW m^{-2} K^{-1}) surfaces showed ≈20% superior HTC even compared to the flat Si surface.

HTC results were affected by surface structures and wetting conditions and the results can be explained by introducing the concept of bubble nucleation temperature (Figure 4b). Bubble

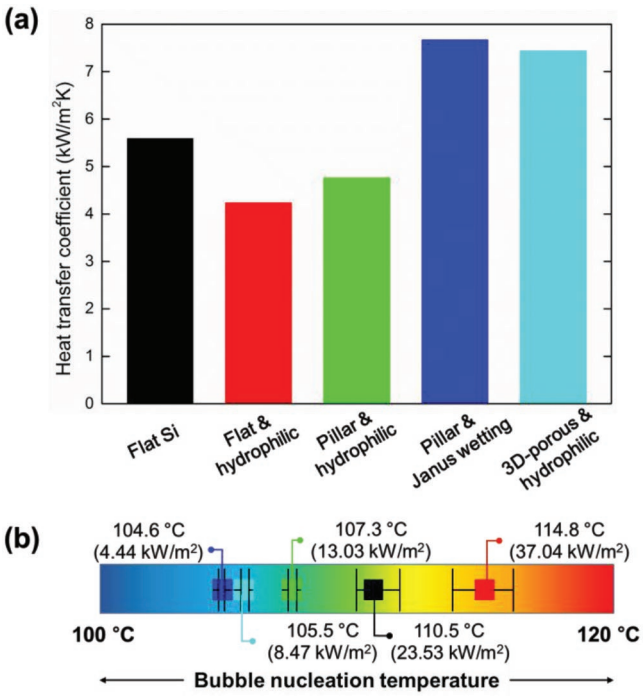

Figure 4. Comparative a) heat transfer efficiencies under heat flux of 100 kW m^{-2} and b) bubble nucleation temperatures and heat fluxes (■ flat Si, ■ flat and hydrophilic, ■ pillar and hydrophilic, ■ pillar and Janus wetting, and ■ 3D-porous and hydrophilic).

nucleation temperature, i.e., temperature at onset of nucleate boiling, is defined as lowest surface temperature which can induce bubble generation, and is measured by gradually reducing surface temperature until all bubbles vanish. Lower nucleation temperature induces more nucleation sites at the same temperature condition, which is strongly related with the bubble generation rate and heat transfer efficiency. All modified surfaces had lower bubble nucleation temperature than flat and hydrophilic one (114.8 °C). Reduced nucleation temperature on microstructures was also reported by other researchers because they act as micron scale cavities on a boiling surface.[40] Compared with pillar and hydrophilic surface, pillar and Janus wetting and 3D-porous and hydrophilic surfaces have hydrophobic patterns and additional macropores, respectively, which could induce much earlier bubble generation.[16,41] Hydrophobic patterns reduce required energy for nucleation and macropores can activate nucleation as seed for nucleation, and both are related with strong affinity for bubbling initiation. Therefore, nucleation temperatures on pillar and Janus wetting (104.6 °C) and 3D-porous and hydrophilic (105.5 °C) structures further decreased than that of pillar and hydrophilic structure (107.3 °C). The early bubble generation resulted in more bubbles at the same heat flux condition, and in turn higher cooling capability with higher HTC could be obtained. This result verifies that the modified AHPCS surface in geometry and chemistry greatly improved the cooling efficiency beyond intrinsic limitation in heat transfer of the material. Therefore, the facile fabrication feasibility of the AHPCS resin may enable to readily devise versatile cooling surface patterns on the electronic components.

Versatile silicate glass surfaces with different geometry (nonporous and 3D-porous micropillars) and the controlled chemistry (hydrophilic, hydrophobic, and Janus wettability) were fabricated to enhance the boiling process by employing advanced, economic inorganic polymer-based soft lithography with universal modification techniques. Eventually, five types of surfaces (flat Si, AHPCS-derived glass: flat and hydrophilic, pillar and hydrophilic, pillar and Janus wetting, 3D-porous and hydrophilic) were analyzed by SEM, contact angle, and droplet impingement test, and their bubble dynamics and the temperature distribution were comparatively investigated by a high speed camera and an IR thermometry. The pillar and Janus wetting and 3D-porous and hydrophilic surfaces showed superior heat transfer efficiency and uniform temperature distribution, compared to the other surfaces, including flat Si wafer. Both selective hydrophobic patterns and macroporous structure induced vigorous bubble generation via facile nucleation at increased active sites. This work verified the feasibility of shape-controlled surfaces for better boiling performance. Finally, it is highly potential to manufacture the durable ceramic like surface textures with excellent cooling efficiency by adopting preceramic resin with superior processability in terms of cost, formability, and durability to metal and silicon based applications.

Experimental Section

Experimental materials and methods as well as additional results are part of the Supporting Information.

Supporting Information

Supporting Information is available from the Wiley Online Library or from the author.

Acknowledgements

H.N. and J.-O.K. contributed equally to this work. Special thanks to Professor Hyungdae Kim in Kyung Hee University for instruction of IR data calibration, Yoon-Ho Hwang in POSTECH for fabrication of Polystyrene beads, Dong-Hyeon Ko in POSTECH for graphical representation, and Toe Kyung Go in Yeungnam University for representation of movies in the Supporting Information. This work was supported by the National Research Foundation of Korea (NRF) grant funded by the Korea government (MSIP) (No. 2008-0061983). This work was supported by the National Research Foundation of Korea (NRF) grant funded by the Korea government (MSIP) (NRF-2015M2A8A2074795).

Received: June 2, 2016
Revised: July 31, 2016
Published online:

[1] S. H. Kim, G. C. Lee, J. Y. Kang, K. Moriyama, M. H. Kim, H. S. Park, *Int. J. Heat Mass Transf.* **2015**, *91*, 1140.
[2] M. A. Darwish, F. Al-Juwayhel, H. K. Abdulaheim, *Desalination* **2006**, *194*, 22.

[3] N. A. Patankar, *Soft Matter* **2010**, *6*, 1613.
[4] G. Hetsroni, A. Mosyak, Z. Segal, G. Ziskind, *Int. J. Heat Mass Transf.* **2002**, *45*, 3275.
[5] A. E. Bergles, *IEEE Trans. Compon. Packag. Technol.* **2003**, *26*, 6.
[6] J. M. Koo, S. Im, L. Jiang, K. E. Goodson, *J. Heat Transf.* **2005**, *127*, 49.
[7] T. M. Anderson, I. Mudawar, *J. Heat Transf.* **1989**, *111*, 752.
[8] S. A. Kalogirou, *Progress Energy Combust. Sci.* **2005**, *31*, 242.
[9] G. Raluy, L. Serra, *J. Uche. Energy* **2006**, *31*, 2361.
[10] J. J. Wei, H. Honda, *Int. J. Heat Mass Transf.* **2003**, *46*, 4059.
[11] H. Jo, D. I. Yu, H. Noh, H. S. Park, M. H. Kim, *Appl. Phys. Lett.* **2015**, *106*, 181602.
[12] R. Chen, M. C. Lu, V. Srinivasan, Z. Wang, H. H. Cho, A. Majumdar, *Nano Lett.* **2009**, *9*, 548.
[13] S. Li, R. Furberg, M. S. Toprak, B. Palm, M. Muhammed, *Adv. Funct. Mater.* **2008**, *18*, 2215.
[14] R. J. Benjamin, A. R. Balakrishnan, *Exp. Therm. Fluid Sci.* **1997**, *15*, 32.
[15] H. T. Phan, N. Caney, P. Marty, S. Colasson, J. Gavillet, *Int. J. Heat Mass Transf.* **2009**, *52*, 5459.
[16] H. Jo, M. Kaviany, S. H. Kim, M. H. Kim, *Int. J. Heat Mass Transf.* **2014**, *71*, 149.
[17] A. R. Betz, J. Jenkins, C. J. Kim, D. Attinger, *Int. J. Heat Mass Transf.* **2013**, *57*, 733.
[18] H. S. Ahn, C. Lee, H. Kim, H. Jo, S. Kang, J. Kim, J. Shin, M. H. Kim, *Nucl. Eng. Des.* **2010**, *204*, 3350.
[19] K. N. Rainey, S. M. You, *J. Heat Transf.* **2000**, *122*, 509.
[20] A. E. Bergles, M. C. Chyu, *J. Heat Transf.* **1982**, *104*, 279.
[21] S. G. Liter, M. Kaviany, *Int. J. Heat Mass Transf.* **2001**, *44*, 4287.
[22] H. Park, H. Cho, J. Kim, J. W. Bang, S. Seo, Y. Rahmawan, D. Y. Lee, K. Y. Suh, *Small* **2014**, *10*, 52.
[23] H. Cho, J. Kim, H. Park, J. W. Bang, M. S. Hyun, Y. Bae, L. Ha, D. Y. Kim, S. M. Kang, T. J. Park, S. Seo, M. Choi, K. Y. Suh, *Nat. Commun.* **2014**, *5*, 3137.
[24] Z. Xiao, A. Wang, D. P. Kim, *J. Mater. Chem.* **2010**, *20*, 2853.
[25] S. Park, D. Lee, H. Ryoo, T. Lim, D. Yang, D. P. Kim, *Chem. Commun.* **2009**, *32*, 4880.
[26] M. Li, D. P. Kim, *Lab Chip* **2011**, *11*, 1126.
[27] Z. Xiao, Y. Zhao, A. Wang, J. Perumal, D. P. Kim, *Lab Chip* **2011**, *11*, 57.
[28] Z. Xiao, A. Wang, J. Perumal, D. P. Kim, *Adv. Funct. Mater.* **2010**, *20*, 1473.
[29] T. H. Yoon, H. J. Lee, J. Yan, D. P. Kim, *J. Ceram. Soc. Jpn.* **2006**, *114*, 473.
[30] D. Ko, W. Ren, J. Kim, J. Wang, H. Wang, S. Sharma, M. Faustini, D. P. Kim, *ACS Nano* **2016**, *10*, 1156.
[31] C. Yang, L. Huang, T. Shen, J. A. Yeh, *Eur. Cells Mater.* **2010**, *20*, 415.
[32] Y. Tang, Q. Zhang, X. Zhan, F. Chen, *Soft Matter* **2015**, *11*, 4540.
[33] T. Wang, H. Chen, K. Liu, Y. Li, P. Xue, Y. Yu, S. Wang, J. Zhang, E. Kumacheva, B. Yang, *Nanoscale* **2014**, *6*, 3846.
[34] S. M. Yang, H. Miguez, G. A. Ozin, *Adv. Funct. Mater.* **2002**, *12*, 425.
[35] S. Young, S. G. Jang, D. Choi, S. Kim, H. K. Yu, *Small* **2006**, *4*, 458.
[36] N. Kurul, M. Z. Podowski, in *Proc. of the 9th Int. Heat Transfer Conf.*, Jerusalem, Israel **1990**, pp. 21–25.
[37] C. Gerardi, J. Buongiorno, L. Hu, T. McKrell, *Int. J. Heat Mass Transf.* **2010**, *53*, 4185.
[38] S. H. Kim, G. C. Lee, J. Y. Kang, K. Moriyama, H. S. Park, M. H. Kim, *Int. J. Heat Mass Trasf.* **2016**, *102*, 756.
[39] C. Y. Han, P. Griffith, *Int. J. Heat Mass Transf.* **1965**, *8*, 887.
[40] H. Honda, J. J. Wei, *Exp. Therm. Fluid Sci.* **2004**, *28*, 159.
[41] C. Li, Z. Wang, P. I. Wang, Y. Peles, N. Koratkar, G. P. Peterson, *Small* **2008**, *4*, 1084.